Moisture Effects on FM300 Structural Film Adhesive: Stress Relaxation, Fracture Toughness, and Dynamic Mechanical Analysis

Gabriel LaPlante,[1] Pearl Lee-Sullivan[2]

[1]*Faculty of Engineering, Université de Moncton, Moncton, New Brunswick E1A 3E9, Canada*
[2]*Department of Mechanical Engineering, University of Waterloo, 200 University Avenue West, Waterloo, Ontario N2L 3G1, Canada*

Received 15 June 2004; accepted 17 August 2004
DOI 10.1002/app.21353
Published online 19 January 2005 in Wiley InterScience (www.interscience.wiley.com).

ABSTRACT: The behavior of cured FM300 epoxy, a structural film adhesive, subjected to partial and full moisture saturation has been evaluated. Three separate but interrelated test methods were used: stress relaxation, fracture toughness, and dynamic mechanical testing. The mechanical response of the epoxy due to increasing moisture content was dependent on the testing method. In stress relaxation testing, the epoxy was plasticized when partially saturated with moisture, but it became more rigid when fully saturated. The plasticization-to-stiffening transition was not observed in the other two test methods. Fracture testing showed that the material toughness increased with increasing moisture concentration: plasticization effects were dominant. Similar changes in the loss modulus were found in dynamic mechanical analysis. We propose that the differences in behavior have been due to differences in load levels and loading rates used in these probing techniques. Stress relaxation testing, at a relatively lower load and loading rate, appeared to be more sensitive to the localized interactions between the absorbed water molecules and the crosslinked structure. Higher loads and loading rates tended to reveal the bulk effects of plasticization only. Nevertheless, there was also strong evidence from glass-transition temperature measurements that these moisture effects were mostly reversible. © 2005 Wiley Periodicals, Inc. J Appl Polym Sci 95: 1285–1294, 2005

Key words: adhesives; relaxation; fracture; toughness; glass transition

INTRODUCTION

Epoxy resins are widely used as adhesives for bonding in the manufacture of aircraft parts. Compared to mechanically fastened joints, bonded joints weigh less because of a reduced number of parts and give a more uniform distribution of stresses along the joint. However, the long-term reliability of adhesive joints subjected to hot and wet conditions has been a cause for concern. Moisture can penetrate into the adhesive and weaken the joint by plasticization or hydrolysis of the adhesive.[1]

The kinematics of water penetration in an epoxy varies with the resin system that is being considered and the exposure conditions.[2–4] In the simplest case, water molecules enter the epoxy without interacting with the molecular segment network. This case can be represented by Fick's law, which assumes that the absorption is a diffusion process only driven by the moisture concentration gradient. Frequently, however, the Fickian model does not adequately represent the absorption process. Such cases are called *non-Fickian*, or *anomalous diffusion*. Carter and Kibler[5] showed that a two-phase (free and bound water) Langmuir model could accurately reproduce non-Fickian water uptake curves. Vanlandingham et al.[6] explained non-Fickian behavior by differences in the crosslink network density, and Soles et al.[7] proposed a mechanism of nanopores blockage by water molecules binding with polar groups. Cai and Weitsman[8] showed that non-Fickian absorption could be explained by changing surface concentrations because of viscoelasticity effects. Roy et al.[9] proposed a model where viscoelasticity is reflected by a time variation of the diffusion coefficient. More recently, LaPlante et al.[10] showed that the absorption of moisture by FM300 epoxy was characterized by time-varying boundary conditions in addition to a significant presence of bound water.

Moisture is known to plasticize epoxies,[11] a phenomenon that translates to a reduction in the glass-transition temperature (T_g) and softening. However, the exact mechanisms responsible for plasticization are still not fully understood, and disagreement persists among researchers.

Correspondence to: P. Lee-Sullivan (pearls@mecheng1.uwaterloo.ca).

Two different approaches are used to explain the plasticization of epoxies by water. The first approach involves the disruption of interchain hydrogen bonds by water molecules. Polar groups in epoxies, such as hydroxyls (OH), have sufficient steric freedom to participate in interchain hydrogen bonding and play a significant role in polymer stiffness below T_g. A disruption of the interchain bonds by water molecules plasticizes the polymer. Adamson[12] studied the swelling of epoxies and concluded that water is present in two states in the epoxy: free water, which resides in the microvoids in the polymer network, and bound water, which disrupts the interchain bonds and causes swelling. Antoon et al.[13] observed the presence of reversible hydrogen bonds between water and the epoxy network with Fourier transform infrared (FTIR) spectroscopy. Recent FTIR work by Musto et al.[14] confirmed the presence of noninteracting water molecules in the epoxy as well as water molecules hydrogen-bound to the epoxy network. Zhou and Lucas,[15] using NMR spectroscopy, reported no evidence of free or tightly bound water molecules in an epoxy network. They observed water in a state between these two extremes and proposed the existence of two types of reversible hydrogen bonds in epoxy systems: type I, which is characterized by a single hydrogen bond, and type II, which results from a double hydrogen bond. They then postulated that type I bonds are responsible for plasticization, whereas type II bonds create secondary crosslinks that stiffen the epoxy network.

The second approach to describe plasticization is based on the polymer–diluent solution concept. In this case, the molecular interactions between water and the epoxy network are considered insignificant. Jelinsky et al.,[16] on the basis of NMR results, concluded that water does not disrupt the interchain hydrogen bonds in epoxy systems. Their findings suggest that plasticization is described by the polymer–diluent model of Kelley and Bueche.[17] Apicella and Nicolais,[4] in a review article, suggested that epoxy resins based on diglycidyl ether of bisphenol A epoxy do not absorb moisture via hydrogen bonding but rather through dilution and adsorption onto the surface of excess free volumes. This contradicted the findings of Antoon et al.[13]

Luo et al.[18] studied the mobility of water in an epoxy with NMR and found a distribution of binding states. However, they found no evidence of truly free or totally immobilized water. Cotugno et al.,[19] with FTIR, also found several states of sorbed water molecules in an epoxy. These recent results suggest that the picture may not be as clear as the presence of two distinct states for water in epoxy networks (free or hydrogen-bound).

Finally, water has also been observed to cause irreversible changes in the molecular structure of epoxies. Xiao et al.,[20] using FTIR and X-ray photoelectron spectroscopy techniques, found evidence of degradation products in the immersion bath used to condition their epoxy specimens. The degradation products were identified as segments of polymer chains resulting from chain scission. In addition, structural changes induced by hygrothermal aging were observed in the epoxy network. These results are an indication that hydrolysis is also a cause of degradation in epoxies.

The effect of moisture on the viscoelastic properties of epoxies has been the subject of previous studies by dynamic mechanical analysis (DMA). Wang and Ploehn[21] observed a direct correlation between moisture uptake and the magnitude of a relaxation process (ω), which appeared as a shoulder on the α-relaxation peak. They also noted a correlation between the apparent activation energy for the lower β relaxation and moisture uptake. Colombini et al.[22] found that water amplified the magnitude of both the β and ω relaxations, the former change being fully reversible but the latter not being completely reversible.

The intent of this study was to investigate the effects of hygrothermal exposure on the behavior of Cytec FM300, a structural film adhesive that is widely used in aerospace applications. Three separate but interrelated sets of experiments were conducted: stress relaxation, fracture toughness, and DMA. Relaxation parameters were found by curve fitting and compared with fracture toughness results. The change in viscoelastic behavior was compared for three different exposure conditions. The reversibility of the moisture effects was also investigated through observation of the characteristic changes in the glass transition.

EXPERIMENTAL

Materials and specimen preparation

Cytec FM300 film adhesive (Cytec Engineered Materials, Havre de Grace, MD) was used in this work. FM300 is a high-temperature epoxy adhesive available either as an unsupported film or with three different polyester carriers, namely, mat, tight knit, or open knit. The adhesive film with an open-knit carrier, FM300-1K, was used for this study.

The epoxy adhesive film, received at a B-stage, was cured into plates by the stacking of several layers to obtain the desired final thickness. The manufacturer's recommended cure for FM300 is at least 1 h at 175°C. To ensure that a full cure was achieved, the plates prepared following this procedure were cured at 175°C for 2 h. Differential scanning calorimetry (DSC) test results showed that adhesive plates cured with this schedule were fully cured.

Two different thickness plates were cured. In the first set, specimens of nominal dimensions 10 × 30 mm were cut from 1.2 mm thick plates prepared as described previously. The surface of the specimens was polished, and the thickness was reduced to 1 mm. These specimens were used for stress relaxation and DMA testing and also to monitor the moisture uptake rate of FM300 epoxy.

The second set was cured for fracture toughness testing. These specimens had nominal dimensions of 105 × 22 mm and were cut from 8 mm thick plates. These specimens were notched as per ASTM D 5045.[23]

The two moisture exposure conditions investigated were a high humidity environment corresponding to 60% relative humidity (RH) and 60°C (the HH condition) and immersion in water at 70°C (the HW condition). HW specimens were immersed in a beaker full of water and kept in a forced convection oven with the temperature maintained at the desired water temperature. The water temperature, as monitored with a thermocouple, was within 69.5 ± 1°C for the whole duration of the conditioning. The HH specimens were conditioned in a Caron 6010 conditioning chamber (Marietta, OH) with a temperature control of ±0.1°C, a uniformity of ±0.3°C, and a humidity control of ±0.2%. The maximum temperature allowed by the chamber was 60°C, which was the exposure temperature used in this case. In addition, unconditioned (U) specimens were used as the reference.

The specimens used for stress relaxation, DMA, and fracture toughness were exposed to the conditioning environment for 6 weeks, removed from this environment, and immediately tested as is. On the basis of previous results,[10] this exposure period yielded a near saturated condition across the thickness of thin specimens (e.g., the stress relaxation and DMA specimens). Because of the thicker fracture toughness specimens, the exposure period was not expected to yield complete saturation of these specimens. However, the moisture would have sufficiently penetrated the specimen in the precrack area to obtain relevant information on the fracture toughness parameter (K_{IC}), which is associated with the initiation of fracture propagation.

To verify the reversibility of the hygrothermal aging effects on the epoxy, additional DMA specimens were used. Only complete immersion was studied: immersion in water at 70°C for 400 and 1100 h. After removal of the conditioned specimens from the water, they were oven-dried at 90°C *in vacuo* for 72 h before testing. Again, U specimens were used as a reference. U specimens were subjected to the same drying schedule to ensure that any difference observed in the material properties were due to the hygrothermal conditioning only and not the effect of drying. The three conditions are referred to as HW400D, HW1100D, and U, respectively.

Experimental techniques and methods

Moisture absorption

The moisture absorption characteristics of the epoxy were determined by the monitoring of the moisture uptake of selected stress relaxation specimens during their conditioning. At intervals during the exposure period, these specimens were weighed with a Sartorius model CP124S (Goettingen, Germany) balance that had a precision of 0.1 mg. Before weighing, the specimens' surfaces were wiped with a lint-free tissue, and the specimens were allowed to stand free at ambient conditions for 1 min.

Stress relaxation

The stress relaxation behavior of the FM300 epoxy was studied with a dynamic mechanical analyzer (model DMA 2980, TA Instruments, New Castle, DE). In a stress relaxation measurement, an instantaneous strain was applied to the specimen and held for a specified length of time during which the decay of the material's elasticity modulus was monitored. Of the various clamp configurations (e.g., tensile, shear, flexure) offered by the DMA 2980 instrument, the small (20-mm support-to-support span) three-point bend clamp was chosen for this investigation. This type of clamp minimizes clamping effects and only requires a small amount of sample material. In addition, this clamp allowed us to use a small specimen thickness (1 mm), which necessitated shorter conditioning times.

In each test, after a temperature equilibration period of 10 min, a constant strain was applied, and the relaxation modulus (E) was recorded for a period of 30 min. The data was collected on a logarithmic time basis, starting with an interval of 1 s/point and increasing by a factor of 1.2 at each data point. To minimize evaporation from the conditioned specimens during the tests, a thin layer of Dow Corning high-vacuum grease (Midland, MI) was applied to the specimen's surface, a technique previously used by Wang and Ploehn.[21] The flexure strain applied to the specimen was 0.1% in all of the tests. This strain limit was verified via a strain sweep test to lie within the material's linear viscoelastic range.

Fracture toughness

Fracture toughness tests were conducted on single-edge notched (SEN) specimens subjected to three-point bending in accordance with ASTM D 5045.[23] The SEN specimens were tested in an Instron model 1332 (Canton, MA) servohydraulic load frame at a loading

rate of 1 mm/min. The distance between supports was 88 mm, that is, four times the sample width as recommended by ASTM D 5045.[23] A data sampling rate of 100 points/s was used to accurately capture the initiation of crack growth.

According to ASTM D 5045,[23] the plane–strain fracture toughness is given by

$$K_{IC} = (P/BW^{0.5})\, f(x) \tag{1}$$

where

$$f(x) = \frac{(2+x)(0.866 + 4.64x - 13.32x^2 + 14.72x^3 - 5.6x^4)}{(1-x)^{3/2}} \tag{2}$$

where P is the load at crack growth (kN), B is the specimen thickness (cm), W is the specimen width (cm), a is the crack length (cm) and $x = a/W$.

Glass transition determination by DMA

The effect of hygrothermal aging on the T_g of FM300 was determined with the DMA 2930 instrument in the multifrequency mode with the same clamp used for the stress relaxation tests. Tests were performed at an oscillation frequency of 1 Hz, and the temperature was ramped from 40 to 220°C at a rate of 3°C/min. We ensured specimen-to-support contact by setting the autostrain to the recommended value of 150%.[24] This means that a static force of 1.5 times, the force required to generate the oscillation was kept during the test. The oscillation amplitude was set at 100 μm, which corresponded to a deformation in the linear viscoelastic range of the material as verified by a strain sweep test.

As for the relaxation tests, high-vacuum grease was used to reduce the loss of moisture during the tests. This technique was not believed to be efficient at high temperatures, and moisture probably evaporated from the specimens during testing. Therefore, it is possible that moisture-induced differences observed in the results between the different specimen conditions were reduced by the evaporation of moisture. Nevertheless, as shown later, the differences observed in T_g between the U, HH, and HW specimens were significant.

RESULTS AND DISCUSSION

Moisture absorption

The results of the moisture uptake experiments are presented in Figure 1, where the data points pertaining to different specimens are identified by different symbols. Five specimens were used for each exposure condition (HW and HW). As expected, Figure 1 shows

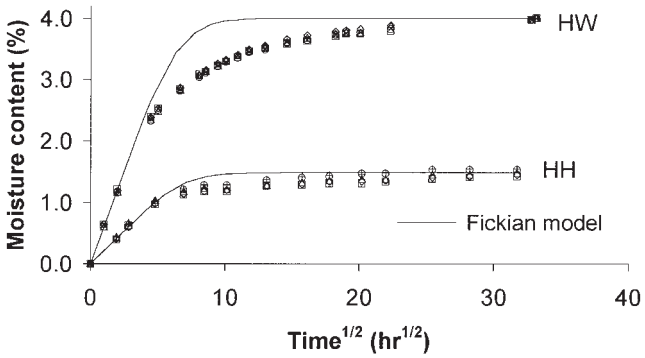

Figure 1 Moisture uptake curves for the HW and HH conditions.

that the initial absorption rate and the final water content were higher for the HW specimen than for the HH specimen. In both cases, however, it appeared that the absorption process did not reach equilibrium during the experimental time frame of more than 1000 h.

The absorption of moisture by a thin plate is assumed one dimensional. The simplest moisture diffusion model in this case is based on Fick's law, which is represented mathematically by[25]

$$\frac{\partial c}{\partial t} = D\,\frac{\partial^2 c}{\partial x^2} \tag{3}$$

where c is the moisture concentration, t is the time, x is the spatial coordinate, and D is the diffusivity. For a plate of thickness $2h$, initially dry and suddenly exposed to an environment with a constant moisture concentration, the average moisture content (M; by weight) inside the plate is given by[26]

$$M(t) = M_\infty\left\{1 - \exp\left[-7.3\left(\frac{Dt}{(2h)^2}\right)^{0.75}\right]\right\} \tag{4}$$

where the subscript ∞ refers to the saturation value.

Predictions from the Fickian model [eq. (4)] are also shown in Figure 1. It was evident by the comparison of these curves to the experimental moisture uptake curves that the absorption was non-Fickian. The nature of this absorption process was studied in more detail by LaPlante et al.[10]

Stress relaxation

The results of the stress relaxation tests are presented in Figure 2. For condition U, the isothermal stress relaxation tests were performed at 40, 70, 100, 120, and 140°C with the same specimen.[27] The test was repeated three times, and the average E values are presented. For the HH and HW conditions, to minimize the potential effects of desorption, each isothermal

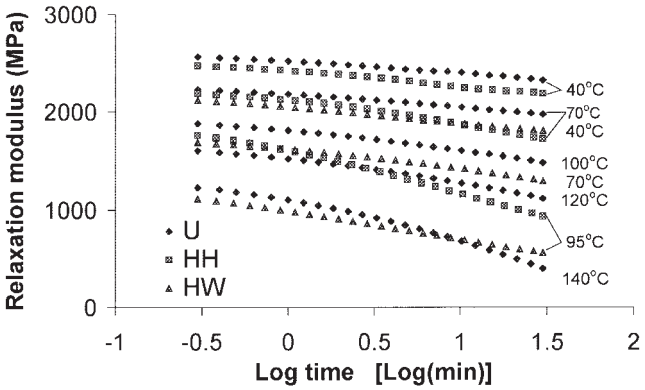

Figure 2 Stress relaxation data for the FM300 epoxy in three conditions: U, HH, and HW.

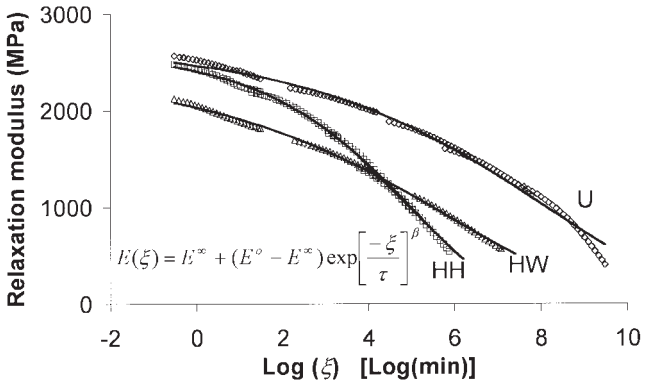

Figure 3 Relaxation master curves for the FM300 epoxy in three conditions: U, HH, and HW.

stress relaxation test was performed with a new specimen. In this case, to improve accuracy and to facilitate time–temperature superposition (TTS), each test was repeated four to five times. The tests were performed at 40, 70, and 95°C only.

The relaxation curves of Figure 2 indicate that for any condition, the overall magnitude of the E decreased as the temperature increased, as expected. A similar trend was found for the moisture content (on the basis of severity of the exposure conditions). At a given temperature, the magnitude of E decreased from the U to the HH condition and finally to HW. The data also show that at elevated temperatures, for example, 70 and 95°C, the modulus of the HH specimens dropped more rapidly with time than that of the HW specimens. This trend suggests that the specimens exposed to 60% RH relaxed more easily than the specimens immersed in water.

TTS

The close relationship between the temperature and the time scale of viscoelastic behavior in a polymer has been generalized into the concept of TTS.[28] On the basis of TTS, the stress relaxation data of Figure 2 were superposed into a single, long-term relaxation curve by the shifting of the individual curves, as shown in Figure 3. The tests performed at 40°C were selected as references in the time shifting operation, and the data corresponding to other temperatures were shifted to the right by amounts equal to $-\log a_T$, where a_T is the shift factor. The a_T values were determined by the visual shifting of the individual curves. This operation is equivalent to the plotting of E against a reduced time variable (ξ), which is defined as[29]

$$\xi = \frac{t}{a_T} \tag{5}$$

where a_T only depends on the temperature.

To improve the appearance of the master curves of Figure 3, some data clipping was performed. The first eight data points of every individual relaxation curve were discarded, corresponding to a truncation of 0.23 min in real testing time at the beginning of each test.

One of the most successful models to describe the stress relaxation behavior of thermosets is a modified version of the Kohlraush–Williams–Watts model.[30] This model, called the *power law model*, is given by[27]

$$E(\xi) = E^{\infty} + (E^{0} - E^{\infty}) \exp\left[\frac{-\xi}{\tau}\right]^{\beta} \tag{6}$$

where E is the relaxation modulus, E^0 is the instantaneous modulus (E at $\xi = 0$), E^{∞} is the relaxed or long-term modulus (E at $\xi = \infty$), τ is the characteristic time constant of the material, and β is a shape factor. The material's relaxation parameters obtained from curve fitting eq. (6) to the experimental data are presented in Table I.

As shown in Table I, the values of E^0 varied only slightly between the specimen conditions, from 2420 to 2690 MPa, which indicated a relative insensitivity of this parameter to hygrothermal aging. E^{∞} was very small for all cases, which meant that the material would eventually have relaxed completely independent of the conditioning. The relaxation constant (τ) however, appeared to be very sensitive to the hygro-

TABLE I
Summary of the Relaxation Parameters Obtained by the Curve Fitting of Eq. (6) to the Experimental Data of Figure 3

Parameter	U	HH	HW
E^0 (MPa)	2690	2630	2420
E^{∞} (MPa)	1.8×10^{-5}	4.4×10^{-7}	3.8×10^{-7}
τ (min)	$1.4 \times 10^{+8}$	$1.1 \times 10^{+5}$	$8.3 \times 10^{+5}$
β	0.130	0.208	0.128
R^2	0.992	0.999	0.999

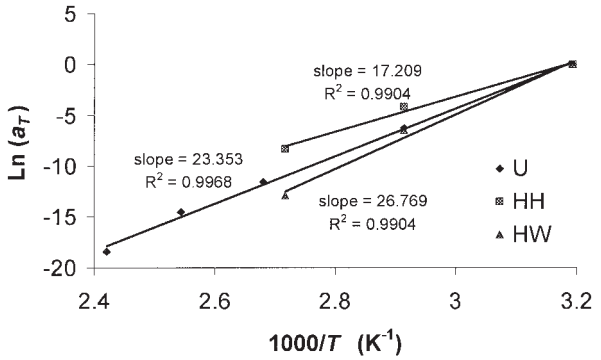

Figure 4 a_T's used in the TTS of Figure 3 for the U, HH, and HW conditions. In each case, the slope of the curve was directly proportional to the activation energy for stress relaxation.

thermal aging condition. The magnitude of τ decreased from 1.4×10^8 min for the U specimen to 1.1×10^5 min after exposure to 60% RH (HH), a difference of three orders of magnitude. Unexpectedly, for specimens immersed in water (HW), τ was equal to 8.3×10^5 min, which was higher than for HH specimens. This behavior suggested that two competing mechanisms acted during the hygrothermal aging of the FM300 epoxy. At low moisture contents, the material relaxed more easily, following plasticization behavior, but when the moisture content exceeded a threshold value, the water molecules started to impede stress relaxation. Moreover, β was very similar, having a value of 0.13, for the U and HW conditions, whereas for the HH condition, it had a value of 0.21. This implied that the relaxation mechanism for U and HW were different than for HH.

Activation energy for stress relaxation

The activation energy for stress relaxation represents the energy barrier that must be overcome for the occurrence of molecular motions causing the relaxation. The stress relaxation, characterized by τ, is a thermally activated process that is governed by the Arrhenius equation:[28]

$$\tau = \tau_0 \exp\left(\frac{\Delta H}{RT}\right) \tag{7}$$

where τ_o is a constant, ΔH is the activation energy, R is the gas constant (8.314 kJ/mol · K), and T is the absolute temperature. If it is assumed that for the temperature range considered, stress relaxation shows a constant activation energy, for two experiments performed at different temperatures[28]

$$\ln \frac{\tau_1}{\tau_2} = \ln a_T = \frac{\Delta H}{R}\left(\frac{1}{T_1} - \frac{1}{T_2}\right) \tag{8}$$

The rearrangement of eq. (8) yields the expression for the activation energy:

$$\Delta H = R\left[\frac{\partial(\ln a_T)}{\partial(1/T)}\right] \tag{9}$$

The bracketed term on the right hand side of eq. (9) represents the slope of the curve in the plot of ln a_T against $1/T$, which is presented in Figure 4. Linear regression curves through the data points are given for each case presented in Figure 4, and the values of R^2 are an indication of the quality of the fit. The activation energy was obtained directly by the multiplication of the slope by R. The resulting activation energies were 194, 143, and 223 kJ/mol for the U, HH, and HW conditions, respectively. These results indicate that a lower energy barrier existed for the relaxation of the HH specimens, which was in agreement with our earlier observation for τ. However, on the basis of the activation energy, the U specimens appeared to relax more easily than the HW specimens, although this was not conclusive because of some uncertainty in the results due to the small number of data points.

Fracture toughness

Typical fracture toughness test results are presented in Figure 5 for the U, HH, and HW conditions. The data presented in Figure 5 was not corrected for displacement offset. The maximum loads reached before crack propagation were 0.33, 0.38, and 0.36 kN for the U, HH, and HW, specimens, respectively. For the U and HH specimens, the loading curves indicated that the crack propagation occurred suddenly, after a linear load increase from 0 to a maximum value. However, in the HW specimen, the crack propagated after a leveling off in the loading curve. Observation of the broken samples revealed that the HW specimen had a

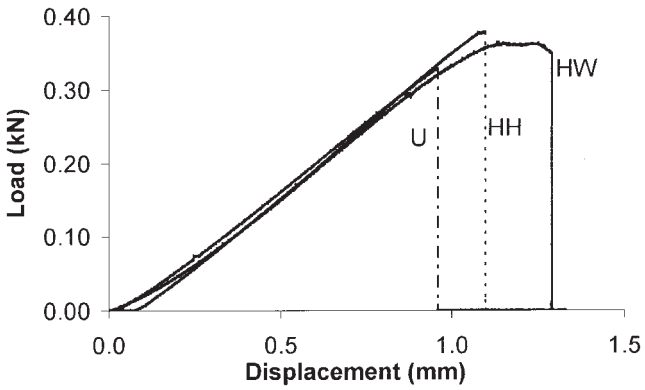

Figure 5 SEN, three-point bending fracture test results. The fracture tests were performed in accordance with ASTM D 5045.[23]

TABLE II
Fracture Toughness Results

Specimen		Moisture content					K_{IC} (MPa. mm$^{1/2}$)		
Condition	No.	(%)	P (kN)	B (cm)	W (cm)	a (cm)	K_{IC}	Average	Standard deviation
U	1	0	0.329	0.872	2.220	1.086	2.605	2.448	0.137
	2	0	0.243	0.738	2.264	1.141	2.357		
	3	0	0.232	0.732	2.278	1.182	2.382		
HH	1	0.942	0.378	0.865	2.245	1.117	3.086	2.948	0.147
	2	1.074	0.281	0.731	2.278	1.161	2.794		
	3	1.082	0.302	0.735	2.263	1.146	2.965		
HW	1	3.13	0.345	0.874	2.235	1.119	2.817	2.818	0.097
	2	3.14	0.364	0.864	2.257	1.110	2.916		
	3	3.22	0.345	0.878	2.233	1.096	2.721		

The fracture tests were performed in accordance with ASTM D 5045[23].

whitish area near the tip of the initial crack, where the crack growth initiated, suggesting the occurrence of crazing. This was not observed in the other two conditions (i.e., HH and U).

Following on ASTM D 5045,[23] the load we used to determine K_{IC} was the maximum load on the loading curve (Fig. 5) within a region defined by the linear portion of the loading curve and a straight line representing an increase of 5% in compliance compared to the first line. In all of the cases presented in this article, this criterion yielded load values practically equal to the maximum loads, and the latter values were used in the calculations. The data presented herein met the plane–strain criteria of ASTM D 5045.[23]

A total of three specimens were tested for each exposure condition, and the resulting fracture toughness results are presented in Table II. The results show that K_{IC} was greater for the HH and HW specimens than for the U specimen. This was expected as a result of the plasticization of the epoxy due to moisture. However, the results clearly indicate that the changes in K_{IC} were not proportional to the moisture content. The increase in moisture content from 0% to about 1% increased K_{IC} from 2.4 to 2.9 MPa $\cdot$ mm$^{1/2}$, respectively, whereas the subsequent increase in moisture content from about 1% to about 3% only resulted in minimal changes in K_{IC} from 2.9 to 2.8 MPa $\cdot$ mm$^{1/2}$.

There was some indication that the K_{IC} values for the HH condition were slightly higher than those for the HW condition, although it was not conclusive because of experimental scatter in the results. This trend would agree with that observed trend in the stress relaxation results, where a higher moisture content resulted in a lower relaxation rate, that is, a lower molecular mobility. However, as shown in Figure 5, the HW specimens had higher ductility than the HH specimens, even though the stiffness changes were minimal.

It is evident from our results why there is still considerable uncertainty in the literature on how moisture causes plasticization behavior in thermosetting polymers. Depending on the experimental technique used, the crosslinked structure responded very differently with increasing moisture concentration. It seemed that at a larger loading scale and rate, plasticizing was more apparent. More localized probing methods, however, would provide a somewhat different view: full moisture saturation may in fact suppress molecular mobility.

Moisture effects on the glass transition

T_g of the epoxy specimens was determined by DMA. Typical DMA test results are shown in Figure 6, where the storage modulus (E'), the loss modulus (E''), and the loss tangent (tan δ) are plotted against temperature. The results for the U specimen showed a peak in E'' around 171°C, whereas the peak in tan δ occurred at 183°C. These peaks were used to define T_g, which was also characterized by a sudden drop in E'. For the HH specimen, T_g based on E'' and tan δ occurred at temperatures of 158 and 179°C, respectively, which were substantially lower than for the U specimen. For the HW specimen, the peaks in E'' and tan δ were shifted even more, to 122 and 177°C, respectively. The average values of T_g for all of the conditions are presented in Table III. The values presented are based on four to five independent tests. Overall, these results show that the peak in E'' was more sensitive to the presence of moisture.

Another main difference among the results of Figure 6 was the widening of the peaks of the E'' and tan δ curves with increasing levels of moisture, particularly for the HW specimen. There was greater molecular mobility at lower temperatures when moisture was present in the epoxy network structure.

Activation energy for the glass transition

The activation energy of the glass transition represents the energy barrier that must be overcome for the oc-

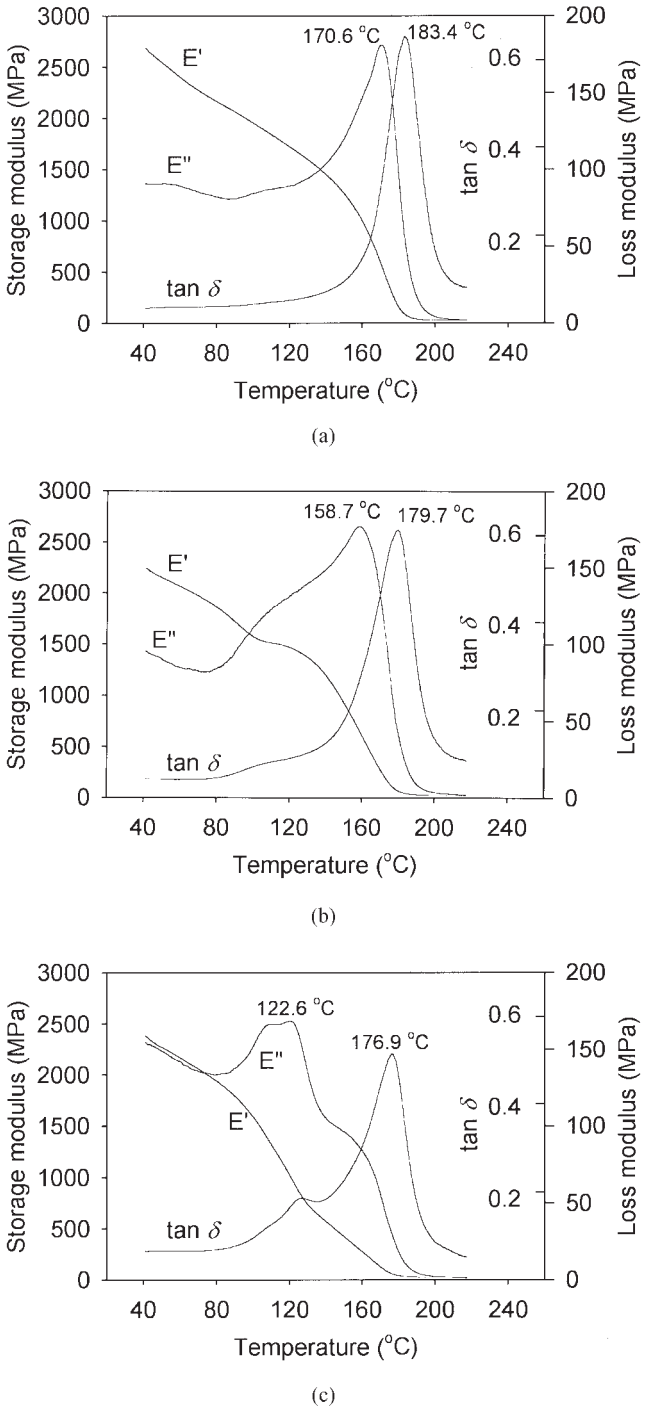

Figure 6 Typical DMA test results at 1 Hz for the (a) U, (b) HH, and (c) HW conditions.

currence of molecular motions causing the transition. The frequency (f) of molecular motions in a polymer obeys the Arrhenius law[28]

$$f = f_0 \exp\left(\frac{-\Delta H}{RT}\right) \tag{10}$$

where f_o is a constant, ΔH is the activation energy, R is the gas constant (8.314 kJ mol$^{-1}\cdot$K^{-1}), and T is the absolute temperature.

TABLE III
T_g as Determined from DMA Tests

	T_g (°C) based on E''			T_g (°C)		
	U	HH	HW	U	HH	HW
Average	171.21	157.05	121.55	182.76	179.29	176.62
Standard deviation	0.88	4.61	1.53	0.46	0.63	0.57

Equation (10) expresses the dependence of T_g on the frequency in a DMA test. For two DMA tests performed at different frequencies, f_1 and f_2, we have

$$\frac{f_1}{f_2} = \frac{\exp(-\Delta H/RT_{g1})}{\exp(-\Delta H/RT_{g2})} \tag{11}$$

When the logarithm is taken and eq. (11) is rearranged,[31] we have

$$\Delta H = -R\left[\frac{\partial(\ln f)}{\partial(1/T_g)}\right] \tag{12}$$

The bracketed term on the right hand side of eq. (12) represents the slope in a plot of ln f against $1/T_g$. With eq. (12), the activation energy of the glass transition was obtained by measurement of the T_g's (based on E'') of samples at the U, HH, and HW conditions at four different test frequencies, namely, 1, 3, 10, and 25 Hz. These results are plotted in Figure 7, where the values of R^2 are an indication of the quality of the linear least squares fit. The activation energies of T_g were found to be 804, 698, and 360 kJ/mol for the U, HH, and HW conditions, respectively. Evidently, the onset of the glass transition was directly facilitated by the presence of moisture. The trend observed in the moisture concentration effects on activation energy for stress relaxation (lowest in the HH case) was not observed in the activation energy for glass transition.

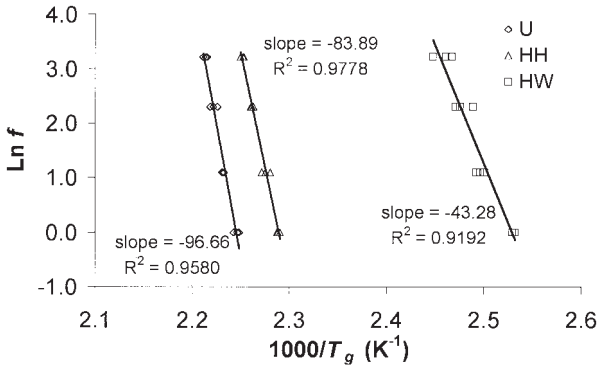

Figure 7 Variation of T_g with the DMA test frequency for the U, HH, and HW conditions. In each case, the slope of the curve was directly proportional to the activation energy of T_g.

TABLE IV
Specimen Weight Before and After Immersion and After Drying

Specimen		Initial	After immersion		After drying	
Condition	No.	weight (g)	Weight (g)	% water	Weight (g)	% water
U	1	0.4159	—	—	0.4161	0.048
U	2	0.4497	—	—	0.4497	0
U	3	0.451	—	—	0.4509	−0.022
HW400D	1	0.4455	0.4623	3.77	0.4457	0.045
HW400D	2	0.4794	0.4973	3.73	0.4796	0.042
HW400D	3	0.4857	0.5039	3.75	0.486	0.062
HW1100D	1	0.4533	0.4717	4.06	0.4534	0.022
HW1100D	2	0.4866	0.506	3.99	0.4866	0
HW1100D	3	0.4648	0.4835	4.02	0.4649	0.022

Reversibility of moisture effects on the glass transition

The values of T_g determined in the previous section were measured with the moisture still present in the specimens. Those results did not reveal whether moisture effects were reversible or due to permanent changes in the epoxy crosslink structure. To investigate this, DMA tests were performed on immersed then dried specimens.

The weights of the specimens resulting from conditioning are summarized in Table IV. After the drying period, the data shows that the amount of residual moisture, expressed in percentage based on the relative weight gain, varied between 0 and 0.06% for the conditioned specimens, which was within the accuracy of the balance. Compared with maximum weight gains of 3.73 to 4.06%, the residual weight gain was minimal.

DMA testing was performed on the conditioned specimens with the same parameters used for the measurement of T_g of the wet specimens. Three specimens were tested for each condition, and the results are summarized in Table V.

By comparing the T_g's (either based on E'' or tan δ) for the three conditions, we found the differences in T_g were only of the order of 4 to 5°C between the U and HW400D/1100D conditions. This residual shift in T_g was less than one-tenth of the shift observed earlier in wet testing, which indicated that the moisture effects on T_g were almost entirely reversible with drying. However, a closer look at the data revealed that there might still have been some irreversible shift, albeit small, and that this shift increased with the length of exposure. The shift in T_g, which was about 4°C for the HW400D condition, increased to about 5°C for HW1100D condition. This was possibly due to trace amounts of residual bound water, which were within the accuracy of the weight measurements, to the permanent rupture of some chemical bonds in the epoxy structure, or to prolonged hygrothermal aging.

CONCLUSIONS

The results of this study show that the non-Fickian moisture absorption behavior of the FM300-1K epoxy was more pronounced for immersed specimens than for those exposed to humid air. Water movement within the network structure was clearly dependent on the RH of the exposure medium.

With regards to the moisture effects, it appeared that the molecular response of the moisture-laden crosslink network was dependent on the probing method used. The loads and loading rates associated with the stress relaxation tests were relatively low compared with that of the fracture toughness tests. At lower loads and loading rates, the plasticization mechanism changed to a stiffening mechanism with increased moisture concentration, but at higher loads, the plasticization effect dominated, regardless of the concentration. A plausible explanation is that moisture concentration affected small-scale localized motions differently than larger scale segmental motions in the crosslink structure, and this was detected by stress relaxation.

Finally, the moisture effects on the mobility of the crosslink network were almost completely reversible on drying. This clearly indicated that the changes associated to moisture exposure were due to plasticization rather than hydrolysis.

Part of the results in this article were presented at the Fourth Canadian International Composites Conference (CANCOM

TABLE V
T_g Results from Specimens Subjected to Hygrothermal Conditioning and Dried

Property	Condition	Test # 1	Test # 2	Test # 3	Average	Standard deviation
T_g (°C) based on E''	U	173.6	172.5	172.8	173.0	0.58
	HW400D	169.0	168.8	168.1	168.6	0.51
	HW1100D	168.4	167.6	167.7	167.9	0.42
T_g (°C) based on tanδ	U	184.0	183.4	183.5	183.6	0.34
	HW400D	180.1	179.6	179.4	179.7	0.37
	HW1100D	179.5	178.4	178.5	178.8	0.59

2003), Ottawa, Canada, August 19–22, 2003. One of the authors (G.L.) was partly supported by a Natural Science and Engineering Research Council postgraduate scholarship and by a research contract with the Canadian Department of National Defence. This author also thanks the Canadian Council for Professional Engineers, the Association of Professional Engineers and Geoscientists of New Brunswick, and the University of New Brunswick for additional scholarships. The authors also thank Ken McRae of the Canadian Department of National Defence for his expert advice.

References

1. Comyn, J. In Durability of Structural Adhesives; Kinloch, A. J., Ed.; Applied Science Publishers: London, 1983; Chapter 3.
2. Weitsman, Y. J. In Fatigue of Composite Materials; Reifsnider, K. L., Ed.; Elsevier: New York, 1990; Chapter 9.
3. Weitsman, Y. J. In Comprehensive Composite Materials; Talreja, R.; Manson, J.-A., Eds.; Elsevier: New York, 2000; Chapter 2.11.
4. Apicella, A.; Nicolais, N. In Advances in Polymer Science; Dusek, K., Ed.; Springer-Verlag: Berlin, 1986; Vol. 72.
5. Carter, H. G.; Kibler, K. G. J Compos Mater 1978, 12, 118.
6. Vanlandingham, M. R.; Eduljee, R. F.; Gillespie, J. W. J Appl Polym Sci 1999, 71, 787.
7. Soles, C. L.; Chang, F. T.; Gidley, D. W.; Yee, A. F. J Polym Sci Part B: Polym Phys 2000, 38, 776.
8. Cai, L.-W.; Weitsman, Y. J Compos Mater 1994, 28, 130.
9. Roy, S.; Xu, W. X.; Park, S. J.; Liechti, K. M. J Appl Mech 2000, 67, 391.
10. LaPlante, G.; Ouriadov, A. V.; Lee-Sullivan, P.; Balcom, B. J. J Appl Polym Sci, accepted.
11. McBrierty, V. J.; Martin, S. J.; Karasz, F. E. J Mol Liq 1999, 80, 179.
12. Adamson, M. J. J Mater Sci 1980, 15, 1736.
13. Antoon, M. K.; Koenig, J. L.; Serafini, T. J Polym Sci Polym Phys Ed 1981, 19, 1567.
14. Musto, P.; Ragosta, G.; Scarinzi, G.; Mascia, L. J Polym Sci Part B: Polym Phys 2002, 40, 922.
15. Zhou, J.; Lucas, J. P. Polymer 1999, 40, 5505.
16. Jelinsky, L. W.; Dumais, J. J.; Cholli, A. L.; Ellis, T. S.; Karasz, F. E. Macromolecules 1985, 18, 1091.
17. Kelley, F. N.; Bueche, F. J Polym Sci 1961, 50, 549.
18. Luo, S.; Leisen, J.; Wong, C. P. J Appl Polym Sci 2002, 85, 1.
19. Cotugno, S.; Larobina, D.; Mensitieri, G.; Musto, P.; Ragosta, G. Polymer 2001, 42, 6431.
20. Xiao, G. Z.; Delamar, M.; Shanahan, M. E. R. J Appl Polym Sci 1997, 65, 449.
21. Wang, J.; Ploehn, H. J. J Appl Polym Sci 1996, 59, 345.
22. Colombini, D.; Martinez-Vega, J. J.; Merle, G. Polymer 2002, 43, 4479.
23. Annual Book of ASTM Standards; ASTM D 5045-93; American Society for Testing and Materials: West Conshohocken, PA, 1995; Vol. 03.01.
24. TA Instruments 2980 Dynamic Mechanical Analyzer Operator's Manual; PN984004.001 Rev C; TA Instruments: New Castle, DE, 1997.
25. Crank, J. The Mathematics of Diffusion; Oxford University Press: London, 1975.
26. Shen, C.; Springer, G. S. J Compos Mater 1976, 10, 2.
27. Hojjatti, M.; Johnston, A.; Denault, J.; Hoa, S. V. In Proceedings of the Third International Composites Conference, CANCOM 2001, Aug 2001, Ottawa, Canada; Hoa, S. V., Johnston, A., Denault, J., Eds., CRC Press: Boca Raton, FL.
28. Ward, I. M.; Hadley, D. W. Mechanical Properties of Solid Polymers; Wiley: Chichester, England, 1993.
29. Chartoff, R. P. In Thermal Characterization of Polymeric Materials, 2nd ed.; Turi, E. A., Ed.; Academic: New York, 1997.
30. Williams, G.; Watts, D. C. Trans Faraday Soc 1970, 66(565), 80.
31. Li, G.; Lee-Sullivan, P.; Thring, R. W. J Therm Anal Cal 2000, 60, 377.